Observations of core-mantle boundary Stoneley modes

Paula Koelemeijer,[1] Arwen Deuss,[1] and Jeroen Ritsema[2]

[1] Core-mantle boundary (CMB) Stoneley modes represent a unique class of normal modes with extremely strong sensitivity to wave speed and density variations in the D" region. We measure splitting functions of eight CMB Stoneley modes using modal spectra from 93 events with $M_w > 7.4$ between 1976 and 2011. The obtained splitting function maps correlate well with the predicted splitting calculated for S20RTS+Crust5.1 structure and the distribution of S_{diff} and P_{diff} travel time anomalies, suggesting that they are robust. We illustrate how our new CMB Stoneley mode splitting functions can be used to estimate density variations in the Earth's lowermost mantle. **Citation:** Koelemeijer, P., A. Deuss, and J. Ritsema (2013), Observations of core-mantle boundary Stoneley modes, *Geophys. Res. Lett.*, *40*, doi:10.1002/grl.50514.

1. Introduction

[2] The D" region is the lowest 200–300 km of the mantle, atop the core-mantle boundary (CMB). D" is characterized by ultra-low-velocity zones (ULVZs), seismic discontinuities, anisotropy, CMB topography, and, most prominently, by large-low-shear-velocity provinces (LLSVPs) below Africa and the Pacific [e.g., *Lay*, 2007; *Garnero and McNamara*, 2008]. The LLSVPs extend hundreds of kilometers both laterally and vertically into the lower mantle [*Ritsema et al.*, 1999]. To assess their effect on mantle dynamics, it is essential to have information on the density variations [*Forte and Mitrovica*, 2001].

[3] Observations of Earth's normal modes have the potential to constrain both wave speed and density variations in the mantle. Previous normal mode analyses suggest an anti-correlation between variations in the seismic shear velocity and density, particularly for the LLSVPs [e.g., *Ishii and Tromp*, 1999; *Trampert et al.*, 2004; *Mosca et al.*, 2012]. These results motivated the modeling of LLSVPs as long-lived "piles" of intrinsically dense material [e.g., *Davaille*, 1999; *McNamara and Zhong*, 2005]. However, it was debated whether some of these density models are robust, as they depend on the regularization and a priori constraints [*Romanowicz*, 2001; *Kuo and Romanowicz*, 2002], and the studied modes have sensitivity to both the upper and lower mantle [*Resovsky and Ritzwoller*, 1999].

[4] Here we revisit normal mode constraints on the density structure of the lower mantle by focusing on Stoneley modes [*Stoneley*, 1924]; a unique class of modes that are confined to solid-liquid interfaces such as the CMB (Figure 1). CMB Stoneley modes have extremely focused sensitivity to structures in D" and the outermost core and hence do not suffer from trade-offs with upper mantle structure. However, they have so far not been observed due to insufficient available data. We present, for the first time, splitting function measurements of CMB Stoneley modes, discuss the robustness of our measurements, and illustrate how they can be used in tomographic inversions to constrain density structures in the lowermost mantle.

2. Normal Modes

[5] Earth's normal modes are standing waves arising along the surface and radius of the Earth. They are observed as clear peaks in the amplitude spectra of several day long seismic recordings of large ($M_w > 7.4$) earthquakes. Modes only exist at discrete frequencies, due to the finite size of the Earth, and are characterized by their radial order n and angular order l. We focus here on spheroidal modes $_nS_l$ which involve P-SV motion. Each normal mode consists of $2l+1$ singlets with azimuthal order m in the range $-l,...,l$. These singlets are degenerate (i.e., have the same frequency) for a spherically symmetric, isotropic, nonrotating Earth model such as the Preliminary Reference Earth Model (PREM) [*Dziewonski and Anderson*, 1981]. Significant splitting of the singlets into different frequencies occurs by the rotation and ellipticity of the Earth and velocity and density heterogeneity, anisotropy, and topography on internal boundaries in the Earth.

[6] Normal mode splitting can be completely described using the splitting function approach introduced by *Woodhouse and Giardini* [1985]. Splitting function coefficients c_{st} are linearly related to the perturbations of the reference Earth model according to:

$$c_{st} = \int_0^a \delta m_{st}(r) K_s(r) \mathrm{d}r + \sum_d \delta h_{st}^d H_s^d \qquad (1)$$

where $\delta m_{st}(r)$ are the spherical harmonic coefficients of angular order s and azimuthal order t to describe Earth structure, including perturbations in S wave velocity (V_s), P wave velocity (V_p), density (ρ), and anisotropy. δh_{st}^d represent topography on discontinuities d, and $K_s(r)$, H_s^d are the associated sensitivity kernels [*Woodhouse*, 1980]. Splitting function maps $F(\theta, \phi)$ are used to visualize splitting functions, i.e.,

$$F(\theta, \phi) = \sum_{s=0}^{2l} \sum_{t=-s}^{s} c_{st} Y_s^t(\theta, \phi) \qquad (2)$$
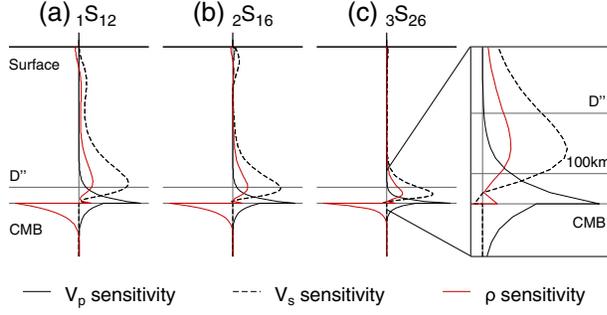
Figure 1. Sensitivity kernels for V_p (solid), V_s (dashed), and ρ (red) for representative CMB Stoneley modes $_nS_l$ and a zoom of the sensitivity in the D" region. Note that the Stoneley mode sensitivity becomes more focused at the CMB with increasing angular order l.

where $Y_s^t(\theta, \phi)$ are the complex spherical harmonics of *Edmonds* [1960]. These maps show the local variation in splitting due to the underlying heterogeneity.

3. Methods and Data

[7] Splitting functions are measured from the inversion of spectra observed for large earthquakes. We make use of a recent normal mode spectra data set of 92 events with $M_w >$ 7.4 for the period 1976–2011 [*Deuss et al.*, 2011, 2013], with the addition of the 2011 Tohoku event ($M_w = 9.0$). Following *Deuss et al.* [2013], we measure the splitting functions using nonlinear iterative least squares inversion [*Tarantola and Valette*, 1982], starting from PREM or predictions for mantle and crust structure. Cross validation is used to determine the errors of our measured coefficients.

[8] Measuring CMB Stoneley modes is complicated as they generally overlap in frequency with a (high-amplitude) fundamental mode with $n = 0$. Hence, we must invert for their splitting functions jointly as previously done for $_1S_{14}$ by *Resovsky and Ritzwoller* [1998]. We also measure the fundamental mode separately to verify that we improve the misfit by including the CMB Stoneley mode. We account for the coupling between fundamental spheroidal and toroidal modes due to Earth's ellipticity and rotation. The misfit is smaller when the CMB Stoneley mode is added (Table 1), which is also visible for individual spectra (Figure 2).

Table 1. Misfit for the Measured Splitting Functions[a]

Modes	PREM	S20	m_{st} i	m_{st} s	N_s	N_{ev}
$_1\mathbf{S_{11}}^s$-$_0S_{15}$-($_0T_{16}$)	1.13	0.54	0.41	0.33	2844	92
$_1\mathbf{S_{12}}^s$-$_0S_{17}$-($_0T_{18}$)	0.85	0.64	0.57	0.53	2312	91
$_1\mathbf{S_{13}}^s$-$_0S_{19}$-($_0T_{20}$)	1.03	0.58	0.39	0.37	1337	91
$_1S_{14}{}^s$-$_0S_{21}$-($_0T_{22}$)	0.93	0.41	0.36	0.30	2983	93
$_1\mathbf{S_{15}}$-$_0S_{23}$-($_0T_{24}$)	1.01	0.38	0.37	0.26	3450	93
$_1\mathbf{S_{16}}$-$_0S_{25}$-($_0T_{26}$)	0.90	0.40	0.74	0.30	2488	92
$_2\mathbf{S_{14}}$-$_0S_{22}$-($_0T_{23}$)	0.93	0.39	0.34	0.29	3343	93
$_2\mathbf{S_{15}}^s$-$_0S_{24}$-($_0T_{25}$)	1.04	0.52	0.69	0.30	2795	92
$_2\mathbf{S_{16}}^s$-$_0S_{26}$-($_0T_{27}$)	1.04	0.40	0.29	0.27	3043	93
$_2\mathbf{S_{25}}^s$-$_3\mathbf{S_{25}}$	1.05	0.78	0.68	0.63	588	76
$_3\mathbf{S_{26}}^s$-$_6S_{15}$-$_9S_{10}$	1.20	0.81	0.68	0.64	751	81

[a]PREM denotes the misfit including only ellipticity and rotation, and S20 denotes the misfit for S20RTS+Crust5.1 synthetics. The final misfit is given for the measurement without (m_{st} i) and with (m_{st} s) the CMB Stoneley mode (denoted by ''s'). The number of spectra (N_s) and events (N_e) is shown. Bold modes correspond to new modes, and modes in brackets are included for rotation and ellipticity coupling.
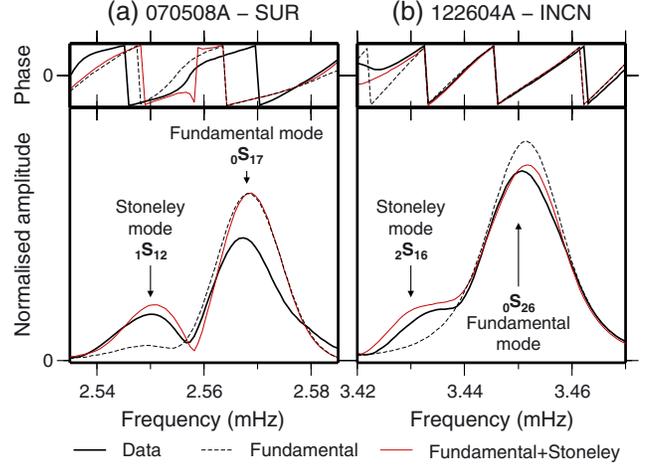
Figure 2. Amplitude and phase spectra for (a) a deep event (Okhotsk, 2008, 615 km, $M_w = 7.7$) at station SUR (South Africa) and (b) a shallow event (Sumatra, 2004, 28.6 km, $M_w = 9.0$) at station INCN (South Korea).

[9] We compare our measurements to predictions for mantle and crust structure, calculated using mantle V_s model S20RTS [*Ritsema et al.*, 1999]. We assume scaling factors of the form $R_p = \delta\ln V_p/\delta\ln V_s = 0.5$ and $R_\rho = \delta\ln\rho/\delta\ln V_s = 0.3$, consistent with previous work [*Karato*, 1993; *Li et al.*, 1991]. The contributions of crustal thickness, surface topography, and water level are calculated using model Crust5.1 [*Mooney et al.*, 1998].

4. Results

4.1. Splitting Function Observations

[10] We have made splitting function measurements of 23 modes in total, including eight CMB Stoneley modes and four other new modes along the same overtone branches ($_1S_{15}$, $_1S_{16}$, $_2S_{14}$ and $_3S_{25}$). In addition, we have measured the associated fundamental modes up to $_0S_{26}$.

[11] The observed splitting function maps (Figure 3) show the "Ring around the Pacific" pattern of high frequencies and pronounced low frequencies at the LLSVPs. Within the "Ring" structure, isolated patches of elevated frequencies are identified, particularly underneath Southeastern Asia and South America. The splitting function maps resemble the predictions for S20RTS+Crust5.1 structure closely. However, individual coefficients such as the c_{20} differ substantially from the predictions (Figure S1 in the supporting information). In addition, the misfit is significantly lower for our measurements (Table 1). We verify using F-test statistics that the misfit reduction due to including the CMB Stoneley mode is significant (90% confidence level). Details on the misfit calculation and F-test can be found in the supplementary online material. Corresponding center frequencies and quality factors for our measurements are in Table 2, and our splitting function coefficients can be found online (Table S1).

4.2. Comparison to S_{diff} and P_{diff} Data

[12] CMB Stoneley modes have similar sensitivity to waves diffracting around the core such as the S_{diff} and P_{diff} phase. We use the travel time anomaly data set from

Observed splitting S20RTS+Crust5.1
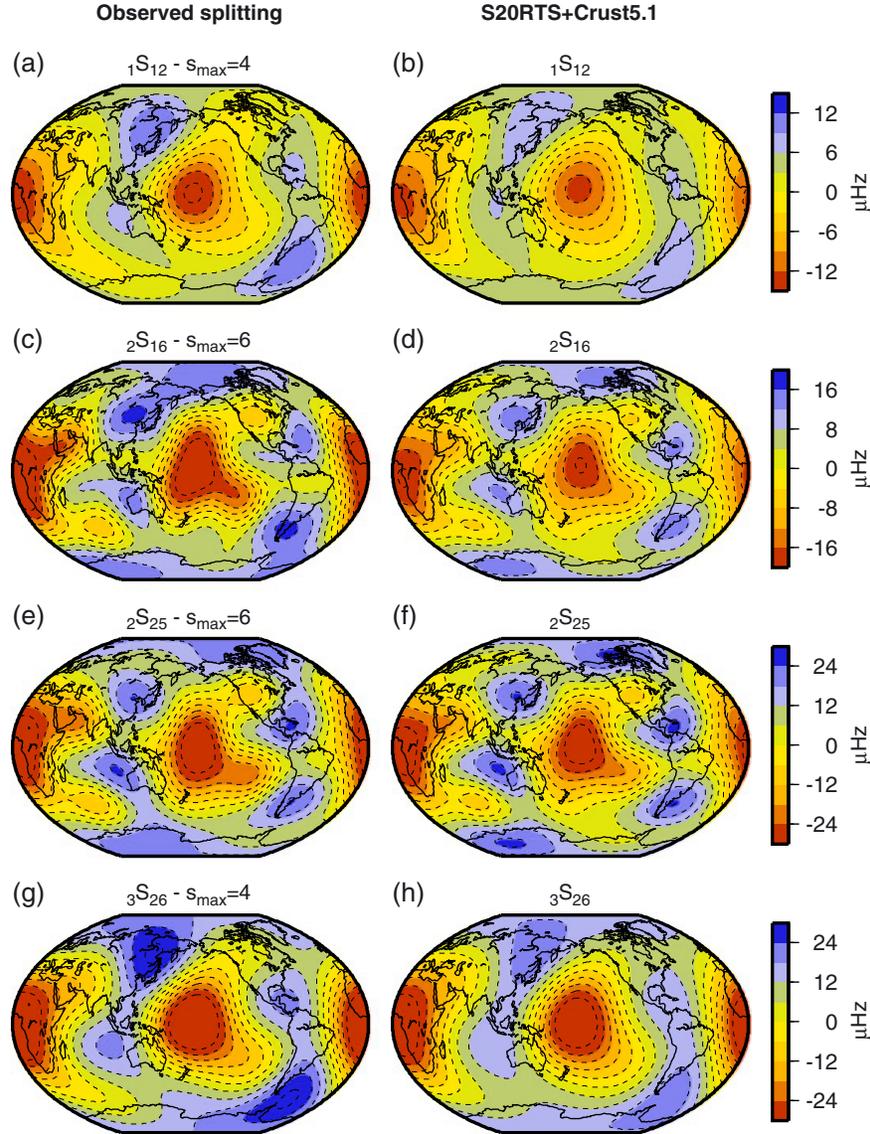
Figure 3. Observed splitting functions for four CMB Stoneley modes and their corresponding predictions for mantle model S20RTS [*Ritsema et al.*, 1999] and crustal model Crust5.1 [*Mooney et al.*, 1998]. The modes have been measured up to angular orders s_{max}.

Ritsema and Van Heijst [2002] obtained for events between 1980 and 2000 with $M_b > 5.9$. The binned data show good coverage in the northern hemisphere but less in the southern hemisphere (Figures 4a–4c). Again, we observe a characteristic "Ring around the Pacific" pattern, becoming even clearer in the even spherical harmonic expansion of the diffracted wave data (Figures 4b–4d), though, some of the southern hemisphere structure could be due to inherent symmetry of the even degree expansion.

[13] The expanded S_{diff} and P_{diff} data and the CMB Stoneley mode splitting functions of $_2S_{25}$ and $_3S_{26}$ have a strong resemblance. The correlation between the modes and S_{diff} data is typically 0.99 and 0.75 for degrees 2 and 4, respectively, whereas the correlation to P_{diff} data is lower at 0.98 and 0.50. This similarity strengthens our confidence in our CMB Stoneley mode measurements. The additional advantage of the normal modes is that they automatically provide coverage in the southern hemisphere.

Table 2. Normal Mode Center Frequencies in µHz and Quality Factors Q for the Modes Measured in This Study Compared With PREM Values[a]

Mode	PREM f	Measured f	PREM Q	Measured Q
$_1\mathbf{S_{11}}^s$	2347.58	2345.64 ± 0.41	374	405 ± 33
$_1\mathbf{S_{12}}^s$	2555.09	2552.55 ± 0.09	365	374 ± 15
$_1\mathbf{S_{13}}^s$	2766.28	2764.32 ± 0.11	345	331 ± 4
$_1\mathbf{S_{14}}^s$	2975.83	2973.73 ± 0.15	293	288 ± 5
$_1S_{15}$	3170.56	3168.96 ± 0.10	203	207 ± 2
$_1S_{16}$	3338.61	3337.58 ± 0.08	166	164 ± 1
$_2S_{14}$	3063.60	3062.25 ± 0.07	188	182 ± 2
$_2\mathbf{S_{15}}^s$	3240.91	3238.69 ± 0.03	258	247 ± 2
$_2\mathbf{S_{16}}^s$	3443.51	3440.80 ± 0.14	354	334 ± 5
$_2\mathbf{S_{25}}^s$	5398.30	5397.21 ± 0.20	366	325 ± 5
$_3S_{25}$	5425.59	5427.09 ± 0.15	207	238 ± 3
$_3\mathbf{S_{26}}^s$	5620.57	5620.73 ± 0.24	402	431 ± 12

[a]Bold modes correspond to new modes.

Traveltime anomalies   **Even degree expansion**
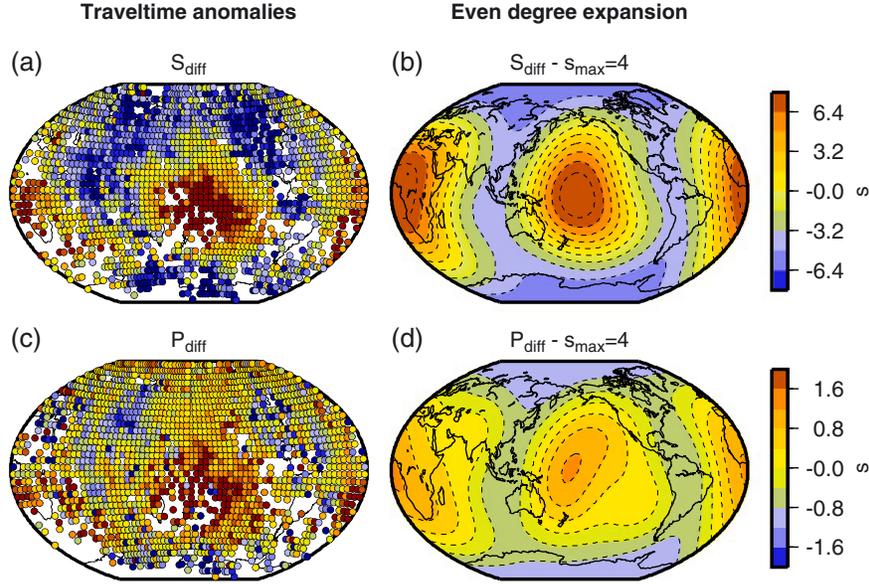
Figure 4. S_{diff} and P_{diff} data for comparison with the CMB Stoneley mode measurements: (a–c) Travel time anomalies with respect to PREM, for epicentral distances of 100–140° plotted at the midpoint of the diffracted path, binned within a 5° cap. (b–d) Even degree spherical harmonic expansion of the travel time data.

4.3. Sensitivity to Density

[14] The sensitivity kernels of the CMB Stoneley modes (Figure 1) show a strong sensitivity to V_p at the CMB, whereas the sensitivity to V_s and ρ is similar and peaks
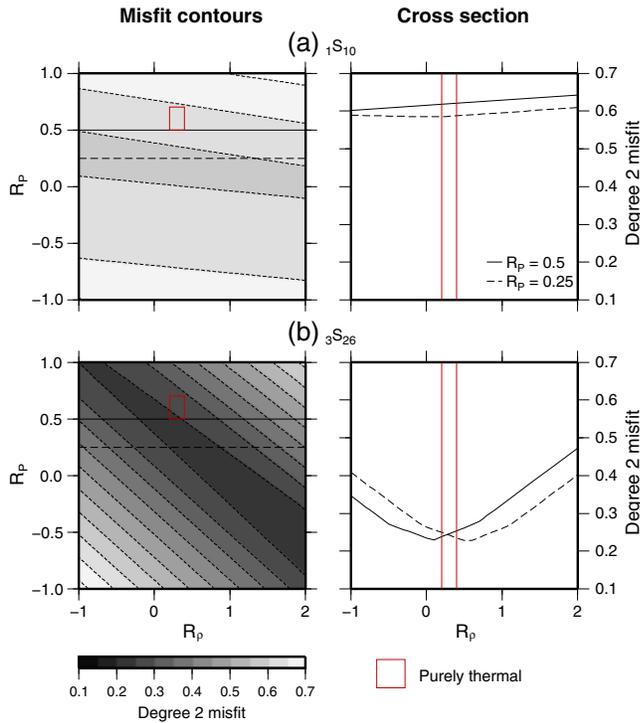
Figure 5. (left) Contour plots of normalized degree 2 misfit between observations and synthetic splitting functions with varying R_P and R_ρ for modes $_1S_{10}$ and $_3S_{26}$. The right panels show a cross section of the misfit versus R_ρ ratio along $R_P = 0.25$ and 0.5. The red box denotes ratios that would be consistent with purely thermal variations [*Karato*, 1993; *Mosca et al.*, 2012].

in the D" above the CMB. Thus, Stoneley modes are useful to constrain R_ρ in the D" which plays an important role in determining the nature of the LLSVPs. We calculate splitting function synthetics using S20RTS and Crust5.1 in which we vary R_p and R_ρ between −1 and 2 for a 300 km thick D" layer. We compute the misfit between the observed and calculated splitting function coefficients for individual modes.

[15] Contour plots of the misfit for $s = 2$ are shown for mode $_1S_{10}$ (previously observed, e.g., *Resovsky and Ritzwoller* [1998] and *Deuss et al.* [2013]) and CMB Stoneley mode $_3S_{26}$ (Figure 5). $_1S_{10}$ can be used to put some constraints on R_P but cannot constrain density variations even though the sensitivity in D" is nonzero. However, $_3S_{26}$ has a strong sensitivity to both R_P and R_ρ, and the same is observed for other CMB Stoneley modes. Assuming values for R_P of 0.5 and 0.25 as a range of possible values [*Karato*, 1993; *Ritsema and Van Heijst*, 2002], we observe for $_3S_{26}$ a best fitting R_ρ of 0.1 and 0.5, respectively, close to the range of ratios that would be consistent with purely thermal variations [e.g., *Karato*, 1993; *Mosca et al.*, 2012]. This suggests that the anticorrelation between density and shear wave velocity might not be required by our new data. However, without good constraints on R_P, we cannot constrain R_ρ accurately. In addition, R_P and R_ρ trade-off with other structures in D" such as CMB topography and ULVZs [*Koelemeijer et al.*, 2012], and therefore, a proper inversion is required to draw any firm conclusions regarding thermal versus thermochemical LLSVPs.

5. Concluding Remarks

[16] Using a data set of 93 large earthquakes, we make robust splitting function observations of eight CMB Stoneley modes. Their splitting function maps correlate well with expanded S_{diff} and P_{diff} data suggesting they are robust. We demonstrate the sensitivity of the Stoneley modes to density variations in the lowermost mantle and illustrate

the trade-off with *P* wave velocity structure. This trade-off can be partially removed when we consider thinner layers (100 km thick) due to the nature of the sensitivity kernels (Figure 1). In addition, a large number of *P* wave sensitive normal mode observations is available [*Deuss et al.*, 2013], and body wave data also provide constraints on R_P. Therefore, when our new measurements are included with these in tomographic inversions, they will help to provide tighter constraints on the density variations in the lowermost mantle.

[18] The Editor thanks Caroline Beghein and an anonymous reviewer for their assistance in evaluating this paper.

References

Davaille, A. (1999), Simultaneous generation of hotspots and superswells by convection in a heterogeneous planetary mantle, *Nature*, *402*(6763), 756–760.

Deuss, A., J. Ritsema, and H. van Heijst (2011), Splitting function measurements for Earth's longest period normal modes using recent large earthquakes, *Geophys. Res. Lett.*, *38*, L04303, doi:10.1029/2010GL046115.

Deuss, A., J. Ritsema, and H. Van Heijst (2013), A new catalogue of normal-mode splitting function measurements up to 10 mHz, *Geophys. J. Int.*, *193*(2), 920–937, doi:10.1093/gji/ggt010.

Dziewonski, A., and D. Anderson (1981), Preliminary reference Earth model, *Phys. Earth Planet. Inter.*, *25*(4), 297–356.

Edmonds, A. (1960), *Angular Momentum in Quantum Mechanics*, Princeton University Press, Princeton, NJ.

Forte, A., and J. Mitrovica (2001), Deep-mantle high-viscosity flow and thermochemical structure inferred from seismic and geodynamic data, *Nature*, *410*(6832), 1049–1056.

Garnero, E., and A. McNamara (2008), Structure and dynamics of Earth's lower mantle, *Science*, *320*(5876), 626.

Ishii, M., and J. Tromp (1999), Normal-mode and free-air gravity constraints on lateral variations in velocity and density of Earth's mantle, *Science*, *285*(5431), 1231.

Karato, S. (1993), Importance of anelasticity in the interpretation of seismic tomography, *Geophys. Res. Lett.*, *20*(15), 1623–1626.

Koelemeijer, P., A. Deuss, and J. Trampert (2012), Normal mode sensitivity to Earth's D" layer and topography on the core–mantle boundary: What we can and cannot see, *Geophys. J. Int.*, *190*, 553–568.

Kuo, C., and B. Romanowicz (2002), On the resolution of density anomalies in the Earth's mantle using spectral fitting of normal-mode data, *Geophys. J. Int.*, *150*(1), 162–179.

Lay, T. (2007), Deep Earth structure – Lower mantle and D", *Treatise on Geophysics*, *1*, 620–654.

Li, X., D. Giardini, and J. Woodhouse (1991), The relative amplitudes of mantle heterogeneity in P velocity, S velocity and density from free-oscillation data, *Geophys. J. Int.*, *105*(3), 649–657.

McNamara, A. K., and S. Zhong (2005), Thermochemical structures beneath Africa and the Pacific Ocean, *Nature*, *437*(7062), 1136–1139.

Mooney, W., G. Laske, and T. Masters (1998), CRUST 5.1: A global crustal model at 5× 5 °, *J. Geophys. Res.*, *103*(B1), 727–747.

Mosca, I., L. Cobden, A. Deuss, J. Ritsema, and J. Trampert (2012), Seismic and mineralogical structures of the lower mantle from probabilistic tomography, *J. Geophys. Res.*, *117*, B06304, doi:10.1029/2011JB008851.

Resovsky, J., and M. Ritzwoller (1999), Regularization uncertainty in density models estimated from normal mode data, *Geophys. Res. Lett.*, *26*(15), 2319–2322.

Resovsky, J. S., and M. H. Ritzwoller (1998), New and refined constraints on three-dimensional Earth structure from normal modes below 3 mHz, *J. Geophys. Res.*, *103*(B1), 783–810.

Ritsema, J., and H. Van Heijst (2002), Constraints on the correlation of P- and S-wave velocity heterogeneity in the mantle from P, PP, PPP and PKPab traveltimes, *Geophys. J. Int.*, *149*(2), 482–489.

Ritsema, J., H. Heijst, and J. Woodhouse (1999), Complex shear wave velocity structure imaged beneath Africa and Iceland, *Science*, *286*(5446), 1925.

Romanowicz, B. (2001), Can we resolve 3D density heterogeneity in the lower mantle? *Geophys. Res. Lett.*, *28*(6), 1107–1110.

Stoneley, R. (1924), Elastic waves at the surface of separation of two solids, *Proc. R. Soc. London, Ser. A, Containing Papers of a Mathematical and Physical Character*, *106*(738), 416–428.

Tarantola, A., and B. Valette (1982), Generalized nonlinear inverse problems solved using the least squares criterion, *Rev. Geophys. Space. Phys.*, *20*(2), 219–232.

Trampert, J., F. Deschamps, J. Resovsky, and D. Yuen (2004), Probabilistic tomography maps chemical heterogeneities throughout the lower mantle, *Science*, *306*(5697), 853.

Wessel, P., and W. Smith (1998), New, improved version of the generic mapping tools released, *Eos Trans. AGU*, *79*, 579–579.

Woodhouse, J. (1980), The coupling and attenuation of nearly resonant multiplets in the Earth's free oscillation spectrum, *Geophys. J. R. Astr. Soc.*, *61*(2), 261–283.

Woodhouse, J., and D. Giardini (1985), Inversion for the splitting function of isolated low order normal mode multiplets, *Eos Trans. AGU*, *66*, 300.